http://dx.doi.org/10.1016/j.ijhydene.2014.10.111

On the tortuosity factor of solid phase in solid oxide fuel cell electrodes

Keqing Zheng[1], Yanxiang Zhang[1,2], Li Li [3], Meng Ni*[,1]

[1] Building Energy Research Group, Department of Building and Real Estate,

The Hong Kong Polytechnic University, Hung Hom, Kowloon, Hong Kong

[2] School of Materials Science and Engineering, Harbin Institute of Technology,

Harbin, Heilongjiang 150001 China

[3] Ability R&D Energy Research Centre, School of Energy and Environment,

City University of Hong Kong, Hong Kong, China

Abstract

Tortuosity factor τ of the solid phase is an important parameter for the accurate prediction of SOFC electrode conductivity. This work investigates the effect of computational domain on τ. The results show that a computational domain with cross section area of 15d*15d (d: particle diameter) is necessary for the calculation of τ when 15% deviation is allowed. The result also validates that the anisotropic property of τ shown in the previous literatures is caused by the insufficient sample size. This study builds a framework for the further study of τ.

Keywords: tortuosity factor; computational domain; anisotropic property

* Corresponding author. Email: bsmengni@polyu.edu.hk;
Tel: (852) 2766 4152 (M. Ni); Fax: (852) 2764 5131.

Nomenclature

d	particle diameter, μm
D_n	computational domain length
j	current density, A/m^2
L_{vox}	voxel length, μm

Greek letters

ϕ	electric potential, V
σ^{eff}	effective conductivity, S/m
σ^0	material intrinsic conductivity, S/m
τ	tortuosity factor
τ_{solid}	tortuosity factor of single phase electrode
τ_{ave}	average value of tortuosity factor in each case
Ψ	volume fraction

1. Introduction

Solid oxide fuel cell (SOFC) has attracted much attention in recent years for its expected high efficiency of power generation, broad fuel flexibility and environmental friendly effect [1]. An SOFC consists of three layers: porous anode, porous cathode, and dense electrolyte. In addition to material development, the ohmic loss of the electrolyte can be significantly reduced by decreasing the electrolyte thickness. It was reported by M. Andersson et al. [2] that only 10% of the total polarization occurred in electrolyte, while the left 30% was in cathode and 60% was in anode for an SOFC with 10 μm YSZ electrolyte and inlet gas temperature at 1010K. As a result, it's more desirable to decrease the polarization losses in electrodes rather than electrolyte to improve the SOFC performance.

Three major kinds of polarization losses exist in SOFC electrodes: the activation polarization loss associated with electrochemical reactions, the ohmic polarization loss related to ion and electron transport and the concentration polarization loss caused by the concentration difference between electrochemical reaction sites and reference conditions. In many early modeling studies on SOFC [3-4], the electrochemical reactions were assumed to occur only in the electrode/electrolyte (E/E) interfaces and thus the ohmic polarization in electrodes was ignored. However, it was found by D.

Chen et al. [5] that the contribution of ohmic polarization to the total electrode polarization was actually significant, especially in the anode side. In SOFC, the effective conductivity (σ^{eff}) of solid phase in electrodes is very important for SOFC actual performance since ohmic polarization loss is mainly determined by the effective conductivity σ^{eff}. In addition, the effective conductivity σ^{eff} also affects the reaction depth, which is a very thin layer from the E/E interface due to the low effective ionic conductivity in electrodes [6].

In SOFC modeling studies, σ^{eff} is usually calculated as follows (for both ionic conducting phase and electronic conducting phase) [7-9]:

$$\sigma^{eff} = \sigma^{0} \frac{\psi}{\tau} \tag{1}$$

where, σ^0 is the material intrinsic conductivity (S/m); Ψ is the volume fraction of the conducting phase (pore phase is included in calculation); τ is the tortuosity factor of the conducting phase. Unlike σ^0 and Ψ, τ is difficult to obtain experimentally and is often directly assumed or used as an adjustable parameter in SOFC modeling studies [10-11]. However, τ plays an influential role in SOFC performance prediction: M. Andersson et al. [2] examined the effect of the tortuosity factor of electrode ionic conducting phase (τ_{io}) on the cell performance with a complete SOFC model and revealed that the current density increased from 3000 A/m^2 to 4050 A/m^2 as the τ_{io} decreased from 10 to 5.

In spite of the significance of τ, studies in this field are limited [12-17] and the values reported in the literatures vary significantly (as shown in Table. 1). H. Iwai et al. [13] reconstructed a Ni/YSZ anode using the focused ion beam scanning electron microscope (FIB-SEM) technique, followed by calculation of τ using random walk method and by solving the steady state diffusion equation in the conducting phase. The volume fraction of their constructed anode was gas/Ni/YSZ=49.6%/25.3%/25.1% and the reported τ of Ni and YSZ (in the Y direction) were 29.45 and 14.82 respectively. By comparison, the τ of Ni reported by N. Vivet et al. [17] was only 10.11 with a similar volume fraction of 26%. Since the Ni phases and YSZ phase are of the same proportion in [13] and [17], it is expected that the τ in each phase should be similar. The large variation of the reported τ was attributed to the insufficient sample size [13-14], yet without any validation. It should

be noted that the unexpected anisotropic property of τ, as another possible consequence of the insufficient sample size was also found in most studies [12-17].

This short communication aims to investigate the effect of the computational domain on τ calculation and its anisotropic property. The three-dimensional (3D) microstructure of conventional binary composite electrode is numerically constructed by a well-validated sphere packing algorithm [18] for its good predictive ability and cost effective property. Finally, τ is obtained by solving charge conservation equations in the conducting phase.

2. Methodology

The detailed procedure for the calculation of τ is designed as follows:

First is to construct the 3D sphere packing structure. A 3D matrix is created and initialized to be zero to simulate the empty container, followed by combination of spherical matrixes to simulate the dropping process of spheres. The voxel length (L_{vox}) in computational domain is 0.05 μm while the particle diameter d is given as 1 μm, i.e. the particle diameter is 20 times of the voxel length (d=20 L_{vox}). The principle of the position selection for a dropped sphere is that the candidate (a spherical vacant domain) with the lowest coordinate in the dropping direction (Z direction) takes precedence. The sphere property is defined by assigning the value of voxel points contained in the sphere, i.e. the ion conducting phase is assigned with positive values, and the electron conducting phase is assigned with negative values. The left part in the computational domain represents gas pores. The generated original structure is shown in Fig. 1.

Second is to dilate spheres to simulate the sintering process. For instance, dilating the electron conducting phase in the original structure (the phase with black color in Fig. 1), the generated network of the dilated electron conducting phase can be found in Fig. 2. By dilating the spheres with 1 voxel length (1.1 times), contact angles of about 34^o can be formed between the adjacent spheres, as shown in Fig. 3. Although this value slightly deviates from the commonly assumed 30^o, it is regarded as acceptable in this study because that an accurate contact angle of 30^o requires a higher resolution accompanied with a much larger computational cost.

Third is to solve the steady state charge conservation equation (Eq. (2)) in each phase with the boundary conditions labeled in Fig.2. Current fluxes j_0 and j_{eff} can be obtained by solving the charge

conservation equation in free space and the dilated specified phase separately. The volume fraction Ψ of the specified phase can be calculated as the ratio of point number in the specified phase to the total point number in the computational domain. Then, the τ can be obtained using Eq. (3).

$$j = \sigma \nabla \phi \tag{2}$$

$$\tau = j_0 \frac{\psi}{j_{eff}} \tag{3}$$

3. Results and discussion

3.1 Model validation

The model calculation is implemented with Matlab®. To conduct model validation, tortuosity factor of the solid phase in single phase electrode τ_{solid} is calculated first. Based on a 5 μm^3 cubic computational domain and by repeating the calculation for 10 times, the average value of τ_{solid} is 3.5 with a maximum deviation of 28%. The literature value 4.36 [19] is also in this range and therefore verifies feasibility of the program. It should be noted that the spheres are dilated to 1.2 times during this calculation to fit with the calculation condition in literature [19].

3.2 Effect of the computational domain

To analyze the effect of the computational domain on τ, 9 cases with different cross section areas (X direction*Y direction) and heights (Z direction) are designed (as listed in Table 2). During calculation, the volume ratio of the ionic conducting phase to the electronic conducting phase is kept as 1:1. Each computational case is repeated for 10 times and the average value of the 10 times calculation results is calculated. Results show that the porosity of the constructed 3D microstructure decreases from 0.41 to 0.28 in the dilating process.

The tortuosity factors based on different computational domains are shown in Fig. 4. The three cases in each figure of Fig. 4 (such as, case 1, 2 and 3) present the difference caused by the different computational domain heights, while in the column direction (such as, case 1, case 4 and case 7) show the effect of the cross section area. It is clearly shown that a larger cross section area decreases the average tortuosity factor (τ_{ave}) as well as the deviation of each calculation. For example, the maximum deviation of case 2 (5d*5d*10d) from its average value (τ_{ave}=7.94) is 57%, but the deviations in case 8 (15d*15d*10d) from their average (τ_{ave}=6.01) are less than 10%. Fig. 4 also shows that a 10d*10d

cross section area guarantees a 30% deviation while a 15*d**15*d* cross section area reduces the deviation to 15%.

Besides, it can be concluded from Fig. 4 that a 5*d* computational domain height (e.g. case 4) always leads to a lower tortuosity factor (τ_{ave}=5.41) than those in the other two cases with the same cross section area but a larger height (τ_{ave}=6.71 in case 5 and τ_{ave}=6.54 in case 6). This phenomenon is reasonable because a lower height is easier to percolate. However, the effect of domain height become weak when computational domain is higher than 10*d*.

According to Fig. 4, a computational domain with a cross section area of 15*d**15*d* is necessary for the calculation of τ, when 15% deviation is allowed. Actually, none of the previous studies [12-17] satisfies this condition. Results in this study indirectly validates that the large variation of τ reported in the previous literatures is caused by the insufficient sample size. However, it should be mentioned that although a large cross section area decreases the deviation of each calculation, it significantly increases the computational cost at the same time.

3.3 Anisotropic property

Based on the 15*d* cubic computational domain (case 9), the tortuosity factors in the X and Y direction (τ_X and τ_Y) are also calculated by changing the boundary conditions to examine the anisotropic property. Considering the two conducting phases in the constructed electrode are of the same fraction, the τ_{ave} in another conducting phase (phase 2) is also calculated for reference. As shown in Fig. 5, the τ_{ave} of phase 1 in X/Y/Z direction are 7.01/6.91/6.48. The average tortuosity factor of the 3 directions is 6.8. Thus the deviation of the τ_{ave} in X/Y/Z direction from this average value is 3.1%/1.7%/4.7%. In the same way, the deviation of τ_{ave} of phase 2 from its average value (=6.9) is 2.5%/3.1%/4.7%. It can be found that only very small deviation (within 5%) exists in the tortuosity factors of the three directions, which is different from the previous findings [12-17]. This result indirectly validates that the anisotropic property of tortuosity factor reported previously is caused by the insufficient computational domain. The small deviation of τ in different directions represented in this work can be attributed to: (1). The intrinsic uncertainty of the random packed electrode structure and (2). the sphere packing algorithm: the lowest coordinate rule used for sphere position selection

guarantes a better connection between spheres in the Z direction, which makes the τ_Z slightly lower than the τ_X and τ_Y.

4. Conclusion

To investigate the tortuosity factor of solid phase in SOFC electrodes so that to predict SOFC performance more precisely, 3D electrode microstructures are constructed using the sphere packing algorithm and dilating method, followed by solving the steady state charge conservation equation in the specified conducting phase and free space to obtain the τ. Results indicate that a computational domain with a cross-section area of 15d*15d is necessary for the calculation of τ (when 15% deviation is allowed). Such a large domain eliminates the large variation and anisotropic property of τ shown in previous reports. It should be noted that the calculation procedure used in this paper is a pure geometric and morphological method and free of any physical property, therefore, it can be safely extended to other similar calculations.

Acknowledgement

This research was supported by a grant (Project Nμmber: PolyU 5326/12E) from Research Grant Council, University Grants Committee, Hong Kong SAR.`

References

[1] Bertei, B. Nucci, C. Nicolella, Microstructural modeling for prediction of transport properties and electrochemical performance in SOFC composite electrodes, Chemical Engineering Science. 101 (2013) 175-190.
[2] M. Andersson, J. Yuan, B. Sundén, SOFC modeling considering electrochemical reactions at the active three phase boundaries, Int. J. Heat Mass Transfer. 55 (2012) 773-788.
[3] M. Ni, M.K.H. Leung, D.Y.C. Leung, Parametric study of solid oxide fuel cell performance, Energy Conversion and Management. 48 (2007) 1525-1535.
[4] S.H. Chan, K.A. Khor, Z.T. Xia, A complete polarization model of a solid oxide fuel cell and its sensitivity to the change of cell component thickness, J. Power Sources. 93 (2001) 130-140.
[5] D. Chen, W. Bi, W. Kong, Z. Lin, Combined micro-scale and macro-scale modeling of the composite electrode of a solid oxide fuel cell, J. Power Sources. 195 (2010) 6598-6610.
[6] Q. Cai, C.S. Adjiman, N.P. Brandon, Investigation of the active thickness of solid oxide fuel cell electrodes using a 3D microstructure model, Electrochim. Acta. 56 (2011) 10809-10819.
[7] J. Deseure, Y. Bultel, L. Dessemond, E. Siebert, Theoretical optimisation of a SOFC composite cathode, Electrochim. Acta. 50 (2005) 2037-2046.
[8] M. Ni, M.K.H. Leung, D.Y.C. Leung, Micro-scale modeling of solid oxide fuel cells with micro-structurally graded electrodes, J. Power Sources. 168 (2007) 369-378.
[9] M.M. Hussain, X. Li, I. Dincer, A nμmerical investigation of modeling an SOFC electrode as two finite layers, Int J Hydrogen Energy. 34 (2009) 3134-3144.
[10] M. Andersson, J. Yuan, B. Sundén, SOFC modeling considering hydrogen and carbon monoxide as electrochemical reactants, J. Power Sources. 232 (2013) 42-54.
[11] M. Chen, Z. Lin, Theoretical models for effective electrical and electrochemical properties of nano-particle infiltrated electrode of solid oxide fuel cell, Int J Hydrogen Energy.

[12] N.S.K. Gunda, H. Choi, A. Berson, B. Kenney, K. Karan, J.G. Pharoah, S.K. Mitra, Focused ion beam-scanning electron microscopy on solid-oxide fuel-cell electrode: Image analysis and computing effective transport properties, J. Power Sources. 196 (2011) 3592-3603.
[13] H. Iwai, N. Shikazono, T. Matsui, H. Teshima, M. Kishimoto, R. Kishida, D. Hayashi, K. Matsuzaki, D. Kanno, M. Saito, H. Muroyama, K. Eguchi, N. Kasagi, H. Yoshida, Quantification of SOFC anode microstructure based on dual beam FIB-SEM technique, J. Power Sources. 195 (2010) 955-961.
[14] M. Kishimoto, K. Miyawaki, H. Iwai, M. Saito, H. Yoshida, Effect of Composition Ratio of Ni-YSZ Anode on Distribution of Effective Three-Phase Boundary and Power Generation Performance, Fuel Cells. 13 (2013) 476-486.
[15] J. Sanyal, G.M. Goldin, H. Zhu, R.J. Kee, A particle-based model for predicting the effective conductivities of composite electrodes, J. Power Sources. 195 (2010) 6671-6679.
[16] N. Vivet, S. Chupin, E. Estrade, T. Piquero, P.L. Pommier, D. Rochais, E. Bruneton, 3D Microstructural characterization of a solid oxide fuel cell anode reconstructed by focused ion beam tomography, J. Power Sources. 196 (2011) 7541-7549.
[17] N. Vivet, S. Chupin, E. Estrade, A. Richard, S. Bonnamy, D. Rochais, E. Bruneton, Effect of Ni content in SOFC Ni-YSZ cermets: A three-dimensional study by FIB-SEM tomography, J. Power Sources. 196 (2011) 9989-9997.
[18] Y. Zhang, C. Xia, M. Ni, Simulation of sintering kinetics and microstructure evolution of composite solid oxide fuel cells electrodes, Int J Hydrogen Energy. 37 (2012) 3392-3402.
[19] K. Rhazaoui, Q. Cai, C.S. Adjiman, N.P. Brandon, Towards the 3D modeling of the effective conductivity of solid oxide fuel cell electrodes - II. Computational parameters, Chemical Engineering Science. 116 (2014) 781-792.

List of Tables and Figures

Table. 1

	[12]	[13]	[14]	[15]	[17]
Microstructure construction	**FIB-SEM**	**FIB-SEM**	**FIB-SEM**	**particle packing**	**FIB-SEM**
Methodology	**Random walk method;**	**Random walk method; Diffusion method**	**Diffusion method**	**Diffusion method**	**Diffusion method**
Computational domain	**Sample A: X: 9.12 µm Y: 4.75 µm Z: 4.08 µm**	**X: 18.6 µm Y: 8.432 µm Z: 6.2 µm**	**X: 18.1 µm Y: 9.72 µm Z: 9.97 µm**	**X: 3.3 µm Y: 3.3 µm Z: 3.3 µm**	**Sample A4: X: 9.12 µm Y: 6.56 µm Z: 5.84 µm**
Voxel	**0.011 µm**		**X: 0.035 µm Y: 0.035 µm Z: 0.062 µm**		**0.01 µm**
Composition	**gas/LSM: 42.5/57.5**	**gas/Ni/YSZ: 49.6/25.3/25.1**	**gas/Ni/YSZ: 36.1/34.2/29.7**		**gas/Ni/YSZ: 41/26/33**
Particle diameter	**0.73 µm**		**Ni: 2 µm YSZ: 1.4 µm**	**0.6 µm**	
Tortuosity factor	**Sample A: gas/LSM: X: 1.398/2.38 Y: 1.43/2.56 Z: 1.89/3.94**	**gas/Ni/YSZ: X:2.03/21.68/27.66 Y:2.06/29.45/14.82 Z:1.83/6.94/9.84**	**gas/Ni/YSZ: X: 3.48/4.91/7.93 Y: 3.04/3.43/5.63 Z: 2.64/3.79/5.39**		**Sample A4: Ni: X: 9.24 Y: 10.11 Z: 39**

Table. 2

Case	Dimensions in three direction: X*Y*Z *d*: particle diameter
1	5*d**5*d**5*d*
2	5*d**5*d**10*d*
3	5*d**5*d**15*d*
4	10*d**10*d**5*d*
5	10*d**10*d**10*d*
6	10*d**10*d**15*d*
7	15*d**15*d**5*d*
8	15*d**15*d**10*d*
9	15*d**15*d**15*d*

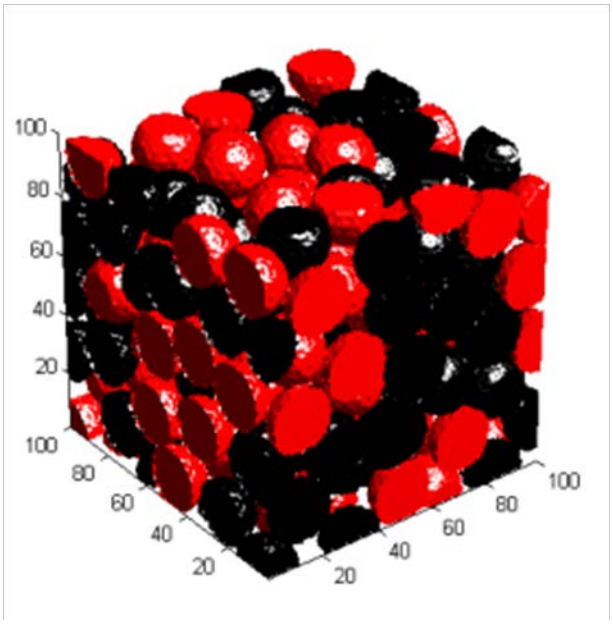

Fig. 1

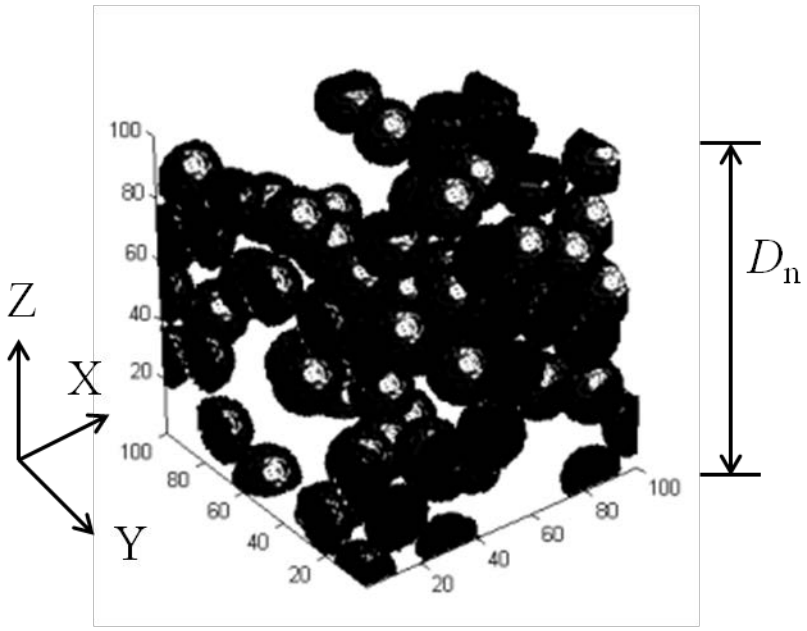

$$Boundary\ conditions\ for\ \tau_Z:$$

$$face\ Z=0, \phi=0;$$

$$face\ Z=D_n, \phi=1;$$

$$other\ \ faces, \nabla\phi=0;$$

Fig. 2

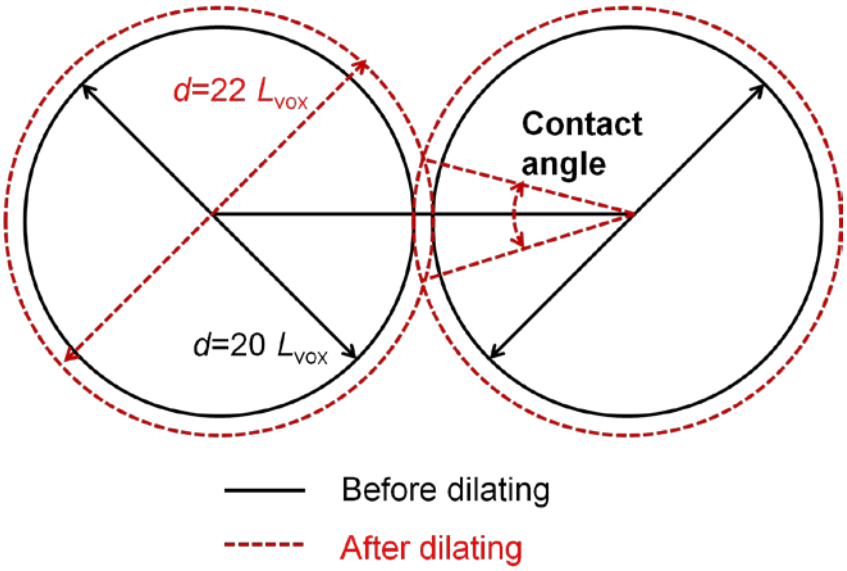
d=22 Lvox
d=20 Lvox
Contact angle
Before dilating
After dilating

Fig. 3

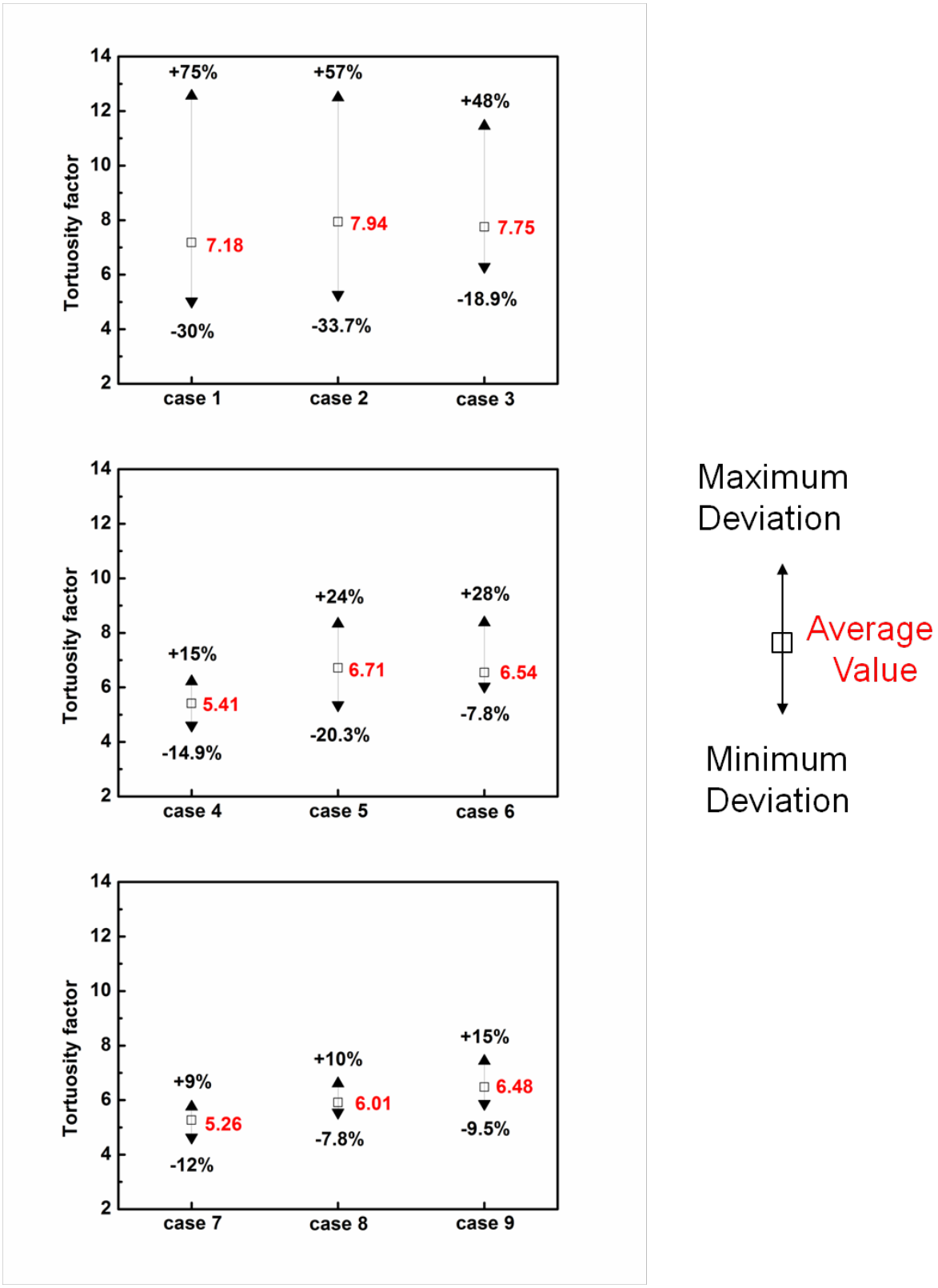

Remark: detailed information of the cases can be found in Table.2 .

Fig. 4

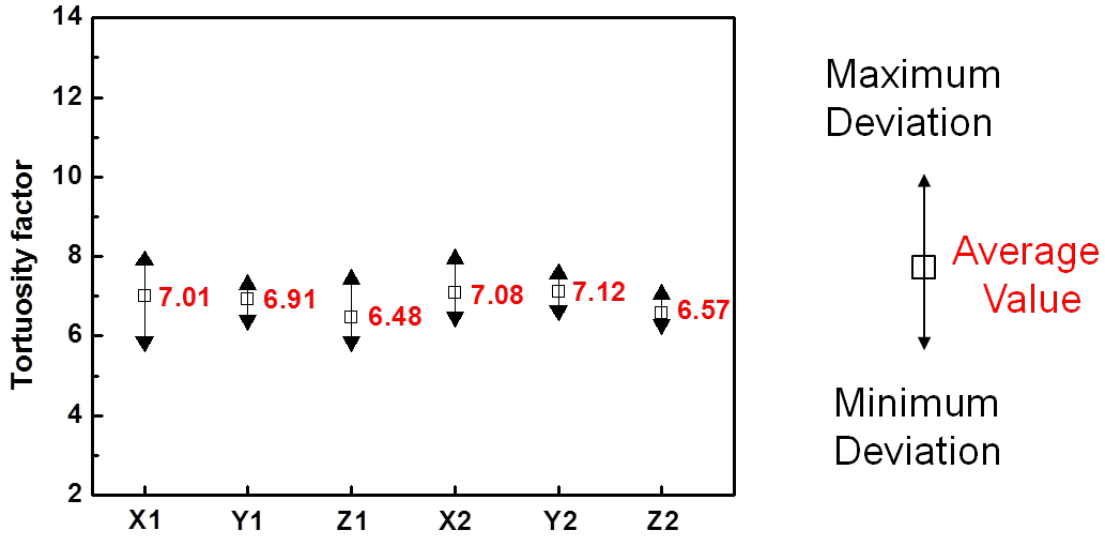
Tortuosity factor
14
12
10
8
6
4
2
7.01
6.91
6.48
7.08
7.12
6.57
X1
Y1
Z1
X2
Y2
Z2
Maximum Deviation
Average Value
Minimum Deviation

Fig. 5